The exponential flow law applied to necking and folding of a ductile layer

Stefan M. Schmalholz[1] and Raymond C. Fletcher[2]

[1]*Institute of Geology and Palaeontology, University of Lausanne,* 1015 *Lausanne, Switzerland. E-mail: stefan.schmalholz@unil.ch*
[2]*Centre for Physics of Geological Processes (PGP), University of Oslo,* 0316 *Oslo, Norway*

GJI Geodynamics and tectonics

SUMMARY

The uniaxial exponential law, $\dot{\varepsilon} = C \exp(a\sigma)$, has been applied to experimental results for steady-state creep, including that of wet and dry olivine, pyroxenite and carbonates, at a deviatoric stress greater than $\sim$100 MPa. Such stress levels likely occur in the upper-mantle lithosphere and middle crust. In a layered rock, in layer-parallel extension or shortening, high deviatoric stress can occur in the stiffest layers, for example, a dolomite layer in fine-grained marble. Under assumptions of isotropy and incompressibility, the uniaxial law yields $D_{ij} = \sqrt{3}C[\exp(a\sqrt{3}J_2^{1/2})/(2J_2^{1/2})]s_{ij}$ where $J_2 = s_{ij}s_{ij}/2$ is an invariant of the deviatoric stress tensor, s_{ij}. Linearization about a homogeneous basic-state of flow yields equations identical in form to those obtained for the familiar power law. This establishes expressions for an effective viscosity, $\bar{\eta} = n_e/2\sqrt{3}a\bar{I}_2^{1/2}$ and stress exponent, $n_e = \ln(2\bar{I}_2^{1/2}/\sqrt{3}C)$, where $\bar{I}_2^{1/2}$ is an invariant of the basic-state deformation rate, $\bar{D}_{ij}$. These results allow application of existing analytical folding and necking solutions for a rock layer of power-law fluid to a rock layer with an exponential flow law. The effective stress exponent for the exponential flow law increases with decreasing temperature, through the dependence of C on the latter and, weakly, with increasing deformation rate. For dry olivine, effective stress exponents are between 10 and 30 for temperatures between 400 and 600°C with little dependence on deformation rate. Finite element simulations employing full non-linear forms of the flow laws show that large strain necking is nearly identical for power law and exponential flow laws. The results suggest that the instability in necking and folding in ductile rock layers can be considerably stronger than inferred from results based on flow laws representing diffusion and dislocation creep. The large values of the effective stress exponent, $n_e > \sim$15, that may be attained for exponential flow laws can account for observed outcrop-scale ductile necking.

Key words: Instability analysis; Creep and deformation; Dynamics of lithosphere and mantle; Folds and folding; Rheology: crust and lithosphere; Mechanics, theory, and modelling.

1 INTRODUCTION

Necking in layer-parallel extension often involves brittle behaviour, such as tensile failure or normal faulting. Continuous pinch-and-swell also occurs and may be a low-strain precursor to such brittle failure. Pinch-and-swell is observed at small scale (e.g. Ramberg 1955; Smith 1977; Schmalholz *et al.* 2008) and may occur early in lithospheric rifting (e.g. Fletcher & Hallet 1983; Ricard & Froidevaux 1986; Bassi & Bonnin 1988; Schmeling 2010) and in slab detachment (e.g. Gerya *et al.* 2004). Folding occurs more frequently than pinch-and-swell, because, as opposed to folding, ductile necking requires strong non-linearity, as expressed, for example, in a large power-law stress exponent, *n*. Both folding and necking have been suggested as mechanisms

for producing regularly spaced linear topographic features on Ganymede (Dombard & McKinnon 2001) and Europa (Dombard & McKinnon 2006).

Folding and necking are prominent elements in the deformation of ductile rocks at all scales (e.g. Biot 1961; Smith 1977; Ricard & Froidevaux 1986; Cloetingh *et al.* 1999; Schmalholz *et al.* 2002; Hutko *et al.* 2006). In plane flow extension or shortening of a single stiff power-law layer embedded in a soft medium, selective amplification at low amplitude is weaker for pinch-and-swell than for folding (e.g. Smith 1977; Schmalholz *et al.* 2008). The relative rate of amplification of a cylindrical pinch-and-swell or fold wavelength component normal to the direction of extension or shortening (Fig. 1) is, for a single stiff layer of power-law fluid embedded in a power-law medium (Fletcher 1974; Smith 1977;
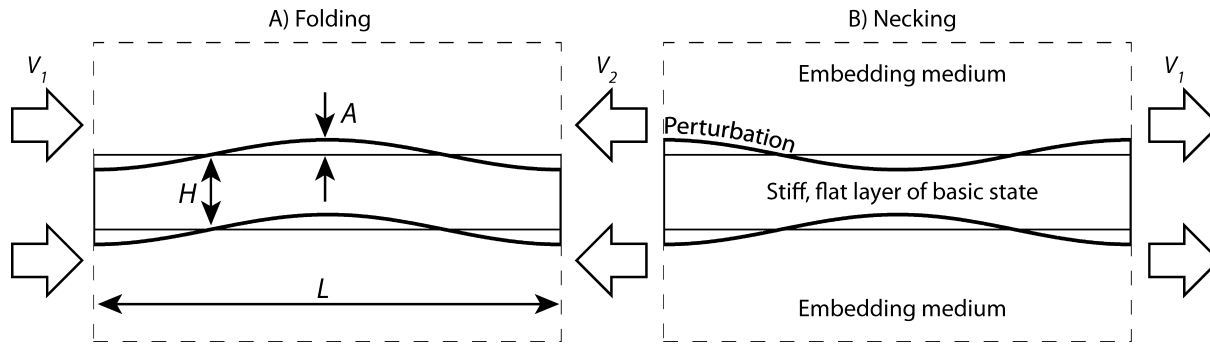
Figure 1. Model set-up and basic parameters for folding (A) and necking (pinch-and-swell, B). A geometrical perturbation in the form of a wavelength component is added to the initially flat layer boundaries to test if the perturbation is stable (growth rate of perturbation, $q < 1$) or unstable ($q > 1$) during layer-parallel shortening (A) or extension (B). A and L are the amplitude and wavelength of the fold or pinch-and-swell wavelength component, respectively and H is the thickness of the initially flat layer. V_1 and V_2 are horizontal (i.e. parallel to the initially flat layer) velocities applied at the lateral, vertical model boundaries. The basic state deformation rate $\bar{D}_{xx} = (V_2 - V_1)/L$.

Schmalholz *et al.* 2008):

$$\left(\frac{1}{A}\right)\frac{dA}{dt} = q\left|\bar{D}_{xx}\right|$$

$$q = -Sgn(\bar{D}_{xx})$$

$$+ \frac{2n(1-R)\,Sgn(\bar{D}_{xx})}{(1-Q^2) \pm \left(\frac{\sqrt{n-1}}{2\sin\beta k}\right)[(1+Q^2)(e^{\alpha k}-e^{-\alpha k}) + 2Q(e^{\alpha k}+e^{-\alpha k})]},$$

$$\tag{1}$$

where $Q = \sqrt{\frac{n}{n_1}}R$, $R = \frac{\bar{\eta}_1}{\bar{\eta}}$, $\alpha = \sqrt{\frac{1}{n}}$, $\beta = \sqrt{1-\frac{1}{n}}$, n and n_1 are the stress exponents of layer and medium, respectively, $\bar{\eta}$ and $\bar{\eta}_1$ are their effective viscosities, t is time, $k = 2\pi(H/L)$, where H is the layer thickness, L is the wavelength and A is the amplitude of the wavelength component (Fig. 1). The positive sign in the denominator applies to a pinch-and-swell perturbation, symmetric about the layer midplane and the negative sign to an asymmetric fold component. The signum function $Sgn(\bar{D}_{xx})$ is +1, 0, or −1 according to whether $\bar{D}_{xx}$ is positive in extension, zero, or negative in shortening. Eq. (1) can, therefore, be applied to all four single-layer instabilities (Smith 1977): folding (shortening with asym-

metric wavelength component), necking (extension with symmetric component), mullion (shortening with symmetric component) and inverse folding (extension with asymmetric component). The maximum of the growth rate q, q_d, is a measure of the strength of instability and L_d/H is the dominant wavelength to thickness ratio.

Amplification, A/A_0 by a factor of 10 in 10 per cent extension, a robust estimate of that required to produce pinch-and-swell structure, requires $q_d = \ln(10)/0.1 = 23$. The aspect ratio of a fold or pinch-and-swell structure produced is roughly estimated by L_d/H (but see Sherwin & Chapple 1968). Contouring q_d and L_d/H in n, R—space for $n_1 = 3$ (Fig. 2) shows that $n \geq 25$ is then required to produce pinch-and-swell structure (Fig. 2b). Values of q_d for folding are significantly larger than for necking at the same n and R (Fig. 2a). From (1), folding can occur in a linear viscous ($n = 1$) layer, whereas necking can only occur (i.e. $q_d > 1$) in a layer with $n > 1$ (Fletcher 1974; Smith 1977; Schmalholz *et al.* 2008), so that pinch-and-swell structure serves as a palaeorheology indicator.

Much experimental creep data (e.g. Carter & Tsenn 1987; Kohlstedt *et al.* 1995) and dislocation theory, is fit by power laws with $n = 3$ to 5. Such rheological behaviour supports folding
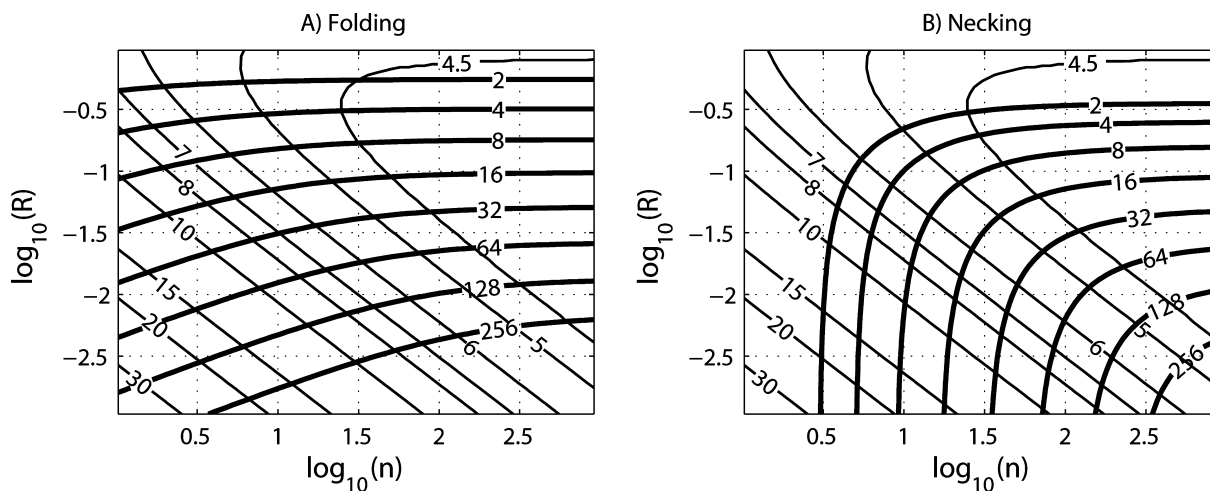
Figure 2. Maximal growth rate, q_d, (thick lines) and dominant wavelength to thickness ratio, L_d/H, (thin lines) from the thick-plate folding and necking (pinch-and-swell) result, eq. (1), as a function of the stress exponent of the layer, n and the effective viscositiy ratio between embedding medium and layer, R (see text for definition of parameters). Stress exponent of the embedding medium, $n_1 = 3$. (A) Values of q_d can be large (>10) even for small values of n. (B) There are two regimes in n, R-space. At large n, q_d depends on R alone; at smaller n, q_d depends on n alone. The marked fall-off of instability with decreasing n is a key difference between the necking instability (B) and the folding instability (A), in which this does not occur.

but these values of n are well below that required for necking (Fig. 2). However, a number of experimental studies (e.g. Rutter 1974; Goetze 1978; Schmid *et al.* 1980; Kirby & Kronenberg 1984; Tsenn & Carter 1987; Davis *et al.* 2008; Katayama & Karato 2008) have shown that at deviatoric stress larger than $\sim$100 MPa, a transition to an exponential law takes place. Some data are fit as well by either law, but, for the power law, require exceptionally large n, for example, $n = 83$ for a clinopyroxenite (Kirby & Kronenberg 1984). An exponential law is required at higher stress for limestone, dolomite, wet and dry olivine and clinopyroxenite. Kirby & Kronenberg (1984) also suggest that the semi-brittle behaviour of rock follows an exponential law. Because the magnitude of deviatoric stress level in a stiff layer may be 10–100 times that in the embedding medium (e.g. Sherwin & Chapple 1968; Trepmann & Stockhert 2009), an exponential law may often be applicable. It likely applies to the olivine-dominated lithospheric mantle at a stress magnitude larger than 100 to 200 MPa (e.g. Goetze 1978; Katayama & Karato 2008).

We will show that the tensor form of the uniaxial exponential flow law, linearized about a basic state of plane flow, has a form identical to that of the power law. The resulting effective stress exponent, n_e, often greatly exceeds values of 3 to 5 for the range of conditions to which this law applies. Existing results for folding and necking of power-law layers, such as (1), immediately apply. Further, large amplitude numerical simulations based on a finite element algorithm solving the full non-linear equations show that the results obtained for the power law and exponential law are nearly identical, if they correspond to identical pairs of effective viscosity and stress exponent determined for the same reference state of deformation.

The use of an effective stress exponent, n_e, in the treatment of unstable growth in localization, as in the initiation of shear zones and of global perturbations, as here, has been made previously by Neurath & Smith (1982), with application to the effect of strain softening in folding and necking and in a more general context, by Montesi & Zuber (2002, 2003).

2 TENSOR FORM OF THE EXPONENTIAL LAW

The exponential law for creep in axial compression can be stated as (e.g. Tsenn & Carter 1987):

$$\dot{\varepsilon} = C \exp(a\sigma). \tag{2}$$

Here $\dot{\varepsilon} > 0$ is the axial rate of shortening, $\sigma > 0$ is the difference of the axial and circumferential normal stress components, where, as opposed to the convention used here, compression is taken as positive and a and C are material constants, C including the exponential temperature dependence. Adopting the sign convention with tension positive:

$$\dot{\varepsilon} = -D_{11}$$
$$\sigma = -(\sigma_{11} - \sigma_{33}), \tag{3}$$

where 1 and 2 = 3 denote the axial and circumferential components, here principal components. Adopting incompressibility and isotropy, (2) may be generalized for arbitrary loading by replacing $\dot{\varepsilon}$ and σ by expressions for them written in terms of the second invariants of the rate of deformation tensor (I_2) and of the deviatoric stress tensor (J_2). For the uniaxial

case:

$$s_{11} = \sigma_{11} - \frac{1}{3}(\sigma_{11} + \sigma_{22} + \sigma_{33}) = \frac{2}{3}(\sigma_{11} - \sigma_{33})$$

$$s_{22} = s_{33} = -\frac{1}{3}(\sigma_{11} - \sigma_{33})$$

$$J_2 = \frac{1}{2}s_{ij}s_{ij} = \frac{1}{2}\left(s_{11}^2 + 2s_{33}^2\right) = \frac{1}{3}(\sigma_{11} - \sigma_{33})^2$$

$$\sigma = \sqrt{3J_2}. \tag{4}$$

Using incompressibility, the axial rate of shortening is obtained from:

$$D_{22} = D_{33} = -\frac{1}{2}D_{11}$$

$$I_2 = \frac{1}{2}\left(D_{11}^2 + D_{22}^2 + D_{33}^2\right) = \frac{3}{4}D_{11}^2$$

$$\dot{\varepsilon} = \frac{2}{\sqrt{3}}\sqrt{I_2}. \tag{5}$$

The exponential flow law in (2) yields:

$$I_2^{1/2} = \frac{\sqrt{3}}{2}C \exp\left(a\sqrt{3}J_2^{1/2}\right) \quad \text{or} \quad \frac{1}{a\sqrt{3}}\ln\left(\frac{2I_2^{1/2}}{\sqrt{3}C}\right) = J_2^{1/2}. \tag{6}$$

For an isotropic and incompressible material, the tensor form of the constitutive relations must be:

$$D_{ij} = F(J_2)s_{ij}. \tag{7}$$

From (7) follows:

$$\frac{1}{2}D_{ij}D_{ij} = [F(J_2)]^2 \frac{1}{2}s_{ij}s_{ij}$$

$$I_2 = [F(J_2)]^2 J_2$$

$$F(J_2) = \frac{I_2^{1/2}}{J_2^{1/2}}. \tag{8}$$

Substituting from (6), the tensor form of the exponential flow law is:

$$D_{ij} = \frac{\sqrt{3}}{2} \frac{C \exp\left(a\sqrt{3}J_2^{1/2}\right)}{J_2^{1/2}}s_{ij}. \tag{9}$$

The inverse relations:

$$s_{ij} = \frac{1}{\sqrt{3}a} \frac{\ln\left(\frac{2}{\sqrt{3}}\frac{I_2^{1/2}}{C}\right)}{I_2^{1/2}}D_{ij} = 2\eta D_{ij} \tag{10}$$

are used in the numerical finite element method to be discussed later. Here, the scalar quantity η may be thought of as the local stress- or rate of deformation-dependent effective viscosity.
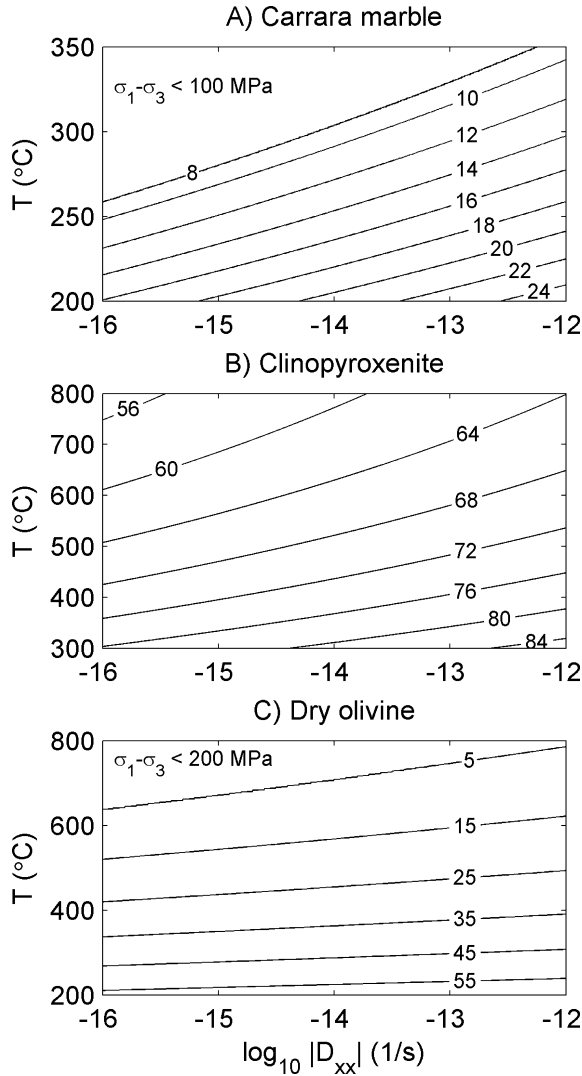
The corresponding result for the power law:

$$\dot{\varepsilon} = A\sigma^n \tag{11}$$

yields:

$$D_{ij} = B\left(J_2^{1/2}\right)^{n-1}s_{ij}$$
$$B = 2(3)^{-(n+1)/2}A. \tag{12}$$

The high stress flow law for Peierl's mechanism, used for olivine based on a Dorn law (Goetze 1978) and often applied to lithospheric deformation, is also an exponential flow law. By the above procedure it becomes:

$$s_{ij} = \frac{\sigma_0}{\sqrt{3}I_2^{1/2}}\left(1 - \left[\frac{RT}{H}\ln\left(\frac{\sqrt{3}\varepsilon_0}{2I_2^{1/2}}\right)\right]^{1/2}\right)D_{ij} \tag{13}$$

Figure 3. Iso-contours of the effective stress exponent, n_e, as a function of absolute shortening rate, $|D_{xx}|$ and temperature, T, for three different rock types. (A) Carrara marble with data from Schmid *et al.* (1980). (B) Clynopyroxenite with data from Kirby & Kronenberg (1984). (C) Dry olivine with data from Molnar & Jones (2004). In (A) and (B) the constant, C, in the exponential flow law, eq. (2), is $C = C_0 \exp(-H/RT)$. In (A) $C_0 = 10^{5.8}$ s^{-1}, $H = 260$ kJ mol^{-1}, $a = 1/11.4$ MPa^{-1} and for (B) $C_0 = 10^{-29}$ s^{-1}, $H = 220$ kJ mol^{-1}, $a = 0.051$ MPa^{-1}. In (C) eq. (23) is used with $\varepsilon_0 = 5.7 \times 10^{11}$ s^{-1}, $H = 525$ kJ mol^{-1} and $\sigma_0 = 8.5$ GPa.

the form obtained by Molnar & Jones (2004). For this flow law, the temperature dependence is explicitly included (caption of Fig. 3 provides material parameters) whereas it is implicitly included in B and C in (9) and (12). The original 1-D form of the high-stress flow law is

$$\dot{\varepsilon} = \varepsilon_0 \exp\left[-\frac{H}{RT}\left(1 - \frac{\sigma}{\sigma_0}\right)^2\right]. \tag{14}$$

However, σ is usually considerably smaller than $\sigma_0 = 8.5$ GPa and (14) can be approximated for $\sigma/\sigma_0 \ll 1$ by

$$\dot{\varepsilon} = \varepsilon_0 \exp\left(-\frac{H}{RT}\right)\exp\left(\frac{2H}{RT}\frac{\sigma}{\sigma_0}\right) \tag{15}$$

equivalent to the standard exponential flow law (2) with $C = \varepsilon_0 \exp(-H/RT)$ and $a = 2H/RT\sigma_0$.

3 LINEARIZATION ABOUT A BASIC STATE OF FLOW: EFFECTIVE VISCOSITY AND STRESS EXPONENT

In the initial phase of instability, selective amplification of the linearly independent components in the perturbed shape of a layer is treated using constitutive relations linearized about a basic state of flow. For the power-law fluid (Fletcher 1974), these relations contain two quantities, an effective viscosity, $\bar{\eta}$ and an effective stress exponent, n_e. If the basic state is plane flow in pure shear, with rate of deformation components $\bar{D}_{xx} = -\bar{D}_{yy}$, $\bar{D}_{xy} = 0$, x and y being coordinates parallel to and normal to layering:

$$\frac{1}{2\bar{\eta}} = B\bar{J}_2^{(n-1)/2}$$

$$n_e = n. \tag{16}$$

In the linearization procedure, we write:

$$D_{ij} = \bar{D}_{ij} + \tilde{D}_{ij}$$

$$s_{ij} = \bar{s}_{ij} + \tilde{s}_{ij}. \tag{17}$$

For a plane perturbing flow associated with a cylindrical perturbation in layer shape, the non-zero perturbing components are:

$$\tilde{D}_{yy} = -\tilde{D}_{xx}$$

$$\tilde{D}_{xy}. \tag{18}$$

Using $s_{xx} = -s_{yy}$:

$$J_2 = \frac{1}{2}\left\{(\bar{s}_{xx} + \tilde{s}_{xx})^2 + (-\bar{s}_{xx} - \tilde{s}_{xx})^2 + 2\tilde{s}_{xy}^2\right\} \cong \bar{s}_{xx}^2 + 2\bar{s}_{xx}\tilde{s}_{xx}$$

$$J_2^{1/2} \cong \sqrt{\bar{s}_{xx}^2}\left(1 + \frac{\tilde{s}_{xx}}{\bar{s}_{xx}}\right) = \bar{J}_2^{1/2} + \bar{J}_2^{1/2}\left(\frac{\tilde{s}_{xx}}{\bar{s}_{xx}}\right). \tag{19}$$

Substituting (17) into (19) and the result into (9) and collecting terms in $\bar{s}_{xx}$ and in $\tilde{s}_{xx}$:

$$\bar{D}_{xx} = \left[\left(\frac{\sqrt{3}C}{2}\right)\frac{\exp\left(a\sqrt{3}\bar{J}_2^{1/2}\right)}{\bar{J}_2^{1/2}}\right]\bar{s}_{xx}$$

$$\tilde{D}_{xx} \cong \left[\left(\frac{\sqrt{3}C}{2}\right)\frac{\exp\left(a\sqrt{3}\bar{J}_2^{1/2}\right)}{\bar{J}_2^{1/2}}\right]\ln\left(\frac{2|\bar{D}_{xx}|}{\sqrt{3}C}\right)\tilde{s}_{xx}. \tag{20}$$

This may also be expressed in the form:

$$s_{xx} \cong 2\bar{\eta}\bar{D}_{xx} + \frac{2\bar{\eta}}{n_e}\tilde{D}_{xx}, \tag{21}$$

where:

$$\bar{\eta} = \frac{1}{2\sqrt{3}a|\bar{D}_{xx}|}\ln\left(\frac{2}{\sqrt{3}}\frac{|\bar{D}_{xx}|}{C}\right)$$

$$n_e = \ln\left(\frac{2}{\sqrt{3}}\frac{|\bar{D}_{xx}|}{C}\right), \tag{22}$$

where $\bar{J}_2^{1/2}$ is expressed in terms of $\bar{I}_2^{1/2} = |\bar{D}_{xx}|$ using (6). Here, the scalar effective viscosity $\bar{\eta}$ depends only on the basic state and is uniform within a layer.

Linearization of the high stress flow law for olivine (13) yields:

$$\bar{\eta} = \frac{\bar{J}_2^{1/2}}{\sqrt{3}\varepsilon_0}\exp\left(\frac{H}{RT}\left(\sqrt{3}\frac{\bar{J}_2^{1/2}}{\sigma_0} - 1\right)^2\right)$$

$$n_e = 2\left(\sqrt{\frac{H}{RT}\ln\left(\frac{\sqrt{3}\varepsilon_0}{2|\bar{D}_{xx}|}\right)} - \ln\left(\frac{\sqrt{3}\varepsilon_0}{2|\bar{D}_{xx}|}\right)\right). \tag{23}$$

Using parameters from laboratory creep experiments, the effective stress exponent, n_e, as a function of $|\bar{D}_{xx}|$ and temperature for Carrara marble, clinopyroxenite and olivine is shown in Fig. 3. n_e decreases with increasing temperature and increases with increasing $|\bar{D}_{xx}|$. For temperatures between 200 and 400°C and $|\bar{D}_{xx}| \sim 10^{-14}\,\mathrm{s}^{-1}$ values of n_e are much larger than those for dislocation creep (Figs 3a and b). For dry olivine, effective stress exponents are between 10 and 30 for temperatures between 400 and 600°C with little dependence on deformation rate (Fig. 3c).

For completeness, we also present the linearized equations for a general basic state flow. For the power-law fluid:

$$\tilde{D}_{ij} \cong \frac{1}{2\bar{\eta}}\left[\tilde{s}_{ij} + (n-1)\left(\frac{\bar{s}_{ij}\bar{s}_{kl}}{\bar{J}_2}\right)\tilde{s}_{kl}\right] \tag{24}$$

with $\bar{\eta}$ given by (16). For the exponential flow law the perturbing relations are:

$$\tilde{D}_{ij} \cong \frac{1}{2\bar{\eta}}\left[\tilde{s}_{ij} + \left(\sqrt{3}a\bar{J}_2^{1/2} - 1\right)\left(\frac{\bar{s}_{ij}\bar{s}_{kl}}{\bar{J}_2}\right)\tilde{s}_{kl}\right] \tag{25}$$

with:

$$\bar{\eta} = \frac{\bar{J}_2^{1/2}}{\sqrt{3}C\exp\left(\sqrt{3}a\bar{J}_2^{1/2}\right)}.$$

The forms of the perturbing relations are identical and, since many results have already been obtained for the power law, we adopt, for the exponential law in the general case:

$$n_e = \sqrt{3}a\bar{J}_2^{1/2} \tag{26}$$

These effective parameters for the exponential flow law also hold for the high stress flow law (Peierl's mechanism) if the approximation (15) is applied.

4 NUMERICAL SIMULATIONS

The relation (1) can be applied to materials obeying an exponential flow law by using the effective viscosity and stress exponent in (22). A numerical FEM solution using the full non-linear flow law produces the same result at small amplitude (Schmalholz *et al.* 2008).

In the Finite Element Method (FEM) algorithm described in Schmalholz *et al.* (2008), the full exponential law (10) was implemented for plane flow. Since the velocity components in the x, y- plane, v_x and v_y, are the principal unknowns in the FEM, we use the kinematic relations to express the invariant in terms of their derivatives:

$$I_2^{1/2} = \sqrt{\frac{1}{2}\left[\left(\frac{\partial v_x}{\partial x}\right)^2 + \left(\frac{\partial v_y}{\partial y}\right)^2 + \frac{1}{2}\left(\frac{\partial v_y}{\partial x} + \frac{\partial v_x}{\partial y}\right)^2\right]}. \tag{27}$$

Both $I_2^{1/2}$ and η are function of the spatially variable velocity components and the resulting non-linear equations are solved iteratively.

Two numerical simulations were performed for layer-parallel extension of a layer with a power-law and with an exponential flow law. The parameters a and C were chosen so that the (basic-state) effective viscosity and effective stress exponent for the exponential law were the same as those of the power law, with parameters B and n, at the basic state extension rate, $|\bar{D}_{xx}|$. Each stiff layer was embedded in a soft power-law medium with stress exponent $n_1 = 3$. For the chosen parameters, $1/R = 40$ and $n_e = 16$, (1) yields $q_d = 10$, indicating that necking is too weak to produce pinch-and-swell
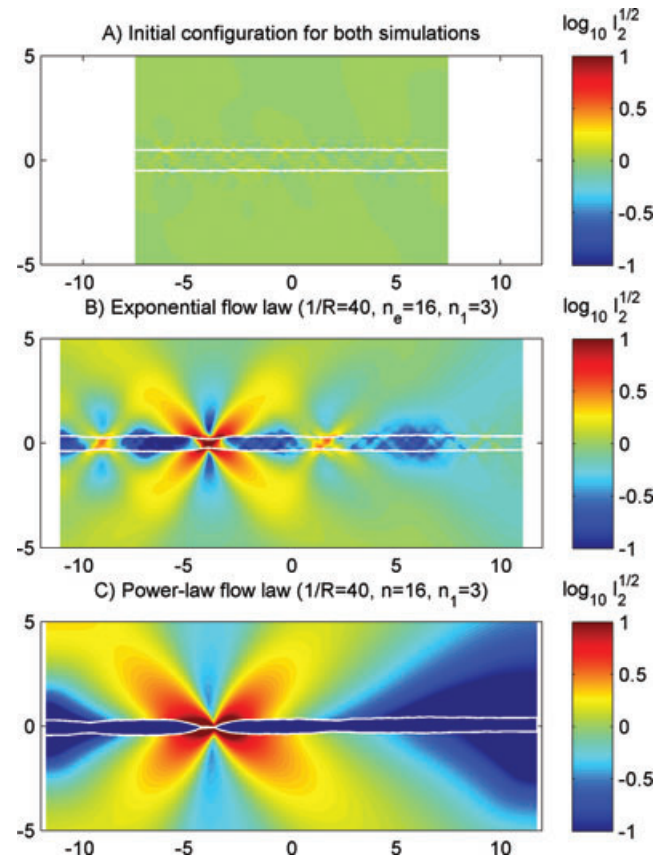
Figure 4. Finite-element simulations of necking generating pinch-and-swell structure. Colours indicate values of $\log_{10}$ of $I_2^{1/2}$ (i.e. second invariant of strain rate tensor). Values are normalized so that $I_2^{1/2} = 1$ (i.e. $\log_{10}(I_2^{1/2}) = 0$) for homogeneous pure shear. The medium surrounding the layer obeys a power-law flow law with $n_1 = 3$. The ratio of effective layer viscosity to matrix viscosity, $1/R = 40$. (A) Initial configuration. (B) Result for layer with exponential flow law with effective stress exponent, $n_e = 16$ at 48 per cent extension. (C) Result for layer with power-law flow law with stress exponent, $n = 16$ at 57 per cent extension.

structure after modest extension. The initial geometry of upper and lower layer surfaces was given a random perturbation with amplitude not exceeding 1/15th of the initial layer thickness (Fig. 4a). The perturbations of the upper and lower layer boundaries were different, but identical for both simulations. After 48 per cent extension (Fig. 4b) amplitude and layer thickness variation are still low, but three necks (or pinches), exhibiting higher strain rate, developed around horizontal positions −9, −4 and 2 with the middle neck showing the largest strain rate. At 57 per cent extension, strain is localized at the highest-amplitude middle neck, while the other two necks were abandoned (Fig. 4c). The strain rate in this neck is more than two orders of magnitude that outside of it. At all stages of extension, the results for the layer obeying an exponential flow law is nearly identical to that for the power-law layer and these are not all shown in Fig. 4.

5 DISCUSSION

In natural layer-parallel shortening or extension, the magnitude of $\sqrt{J_2}$ in the weaker, embedding rock is likely a few to a few tens of MPa. If it is 10 to 100 times larger in the stiff layer, a range of a few hundreds of MPa up to 1000 MPa is attained. In support of this,

Trepmann & Stockhert (2009) interpreted the microfabric of folded quartz veins in greywacke, using experimentally derived relations, to estimate stress in the greywackes less than a few tens of MPa and stress in the quartz vein of a few hundred MPa.

Folding instability occurs in both linear viscous and power-law layers, whereas necking instability only occurs in power-law layers (e.g. Smith 1977) and q_d is bounded above by $n-1$, as may be found from (1) (e.g. Schmalholz *et al.* 2008). Hence, localized ductile necking and regular pinch-and-swell structure can only occur for large values of n_e (e.g. Schmalholz *et al.* 2008). Conversely, the effective rheological behaviour of a rock layer exhibiting either of these structures is likely better described by a high stress, exponential flow law, or by some other plastic or semi-brittle flow law and not by a power law for diffusion creep or for dislocation creep with a stress exponent in the range 1 to 5. Pinch-and-swell structure could form if significant strain softening, as might be due to grain size reduction, takes place in the pinches (e.g. Neurath & Smith 1982). Our results indicate that localized ductile necking can occur for values of $n_e > \sim 15$ whereas regular pinch-and-swell structure likely requires $n_e > \sim 23$ (results not shown here).

We have only considered isotropic flow laws because in the literature experimental data on rock creep which allows establishing anisotropic flow laws are sparse (e.g. Kronenberg *et al.* 1990; Shea & Kronenberg 1993). Formulations of constitutive relations for anisotropic power-law media and application to rock folding have been given in, for example, Fletcher (2005) and Kocher *et al.* (2006). Since many rocks are anisotropic more work in this direction is desirable.

6 CONCLUSIONS

The tensor form for a uniaxial exponential flow law determined in creep experiments was derived. The linearized form is identical to that of a power-law flow law and, correspondingly, an effective viscosity and an effective stress exponent, n_e, may be identified. Substitution of these into analytical solutions for folding and necking originally derived for a power-law flow law then yields equivalent results for the exponential flow law.

Calculation of n_e using creep data for several rocks shows that values of n_e can be considerably larger than 5 for strain rates $\sim 10^{-14}\,\mathrm{s}^{-1}$ and crustal and upper lithospheric mantle temperatures of 200 to 600°C, depending on rock type.

2-D finite element simulations employing the full non-linear exponential and power-law flow laws show that the large strain results in layer extension are nearly identical for both if the corresponding (basic-state) effective viscosity and effective stress exponent are the same. The simulations also show that localized ductile necking will develop for $n_e = 16$ and an effective viscosity ratio of $1/R = 40$ for a total extension less than 100 per cent.

Our results suggest that instability to folding and necking of rock layers composed of limestone, dolomite, clinopyroxene and wet and dry olivine, among others, can be considerably stronger than is inferred from solutions based on flow laws representing diffusion and dislocation creep, for which stress exponents lie in the range from 1 to 5. Consequently, both folding and continuous necking may play a role in initiating structures in continent-continent collision, lithospheric shortening and stretching, rifting or slab detachment, prior to the stage in which localization takes place. Creep behaviour following an exponential flow law, admitting large effective stress exponents, may likewise be inferred to have taken place when small-scale pinch-and-swell structure is observed.

REFERENCES

Bassi, G. & Bonnin, J., 1988. Rheological modeling and deformation instability of lithosphere under extension, *Geophys. J.-Oxford,* **93**(3), 485–504.

Biot, M.A., 1961. Theory of folding of stratified viscoelastic media and its implications in tectonics and orogenesis, *Geol. Soc. Am. Bull.,* **72**(11), 1595–1620.

Carter, N.L. & Tsenn, M.C., 1987. Flow properties of continental lithosphere, *Tectonophysics,* **136**, 27–63.

Cloetingh, S., Burov, E. & Poliakov, A., 1999. Lithosphere folding: primary response to compression? (from central Asia to Paris basin), *Tectonics,* **18**(6), 1064–1083.

Davis, N.E., Kronenberg, A.K. & Newman, J., 2008. Plasticity and diffusion creep of dolomite, *Tectonophysics,* **456**(3–4), 127–146.

Dombard, A.J. & McKinnon, W.B., 2001. Formation of grooved terrain on Ganymede: extensional instability mediated by cold, superplastic creep, *Icarus,* **154**(2), 321–336.

Dombard, A.J. & McKinnon, W.B., 2006. Folding of Europa's icy lithosphere: an analysis of viscous-plastic buckling and subsequent topographic relaxation, *J. Struct. Geol.,* **28**(12), 2259–2269.

Fletcher, R.C., 1974. Wavelength selection in the folding of a single layer with power-law rheology, *Am. J. Sci.,* **274**(11), 1029–1043.

Fletcher, R.C., 2005. Instability of an anisotropic power-law fluid in a basic state of plane flow, *J. Struct. Geol.,* **27,** 1055–1067.

Fletcher, R.C. & Hallet, B., 1983. Unstable extension of the lithosphere – a mechanical model for basin-and-range structure, *J. geophys. Res.,* **88**(NB9), 7457–7466.

Gerya, T.V., Yuen, D.A. & Maresch, W.V., 2004. Thermomechanical modelling of slab detachment, *Earth planet. Sci. Lett.,* **226**, 101–116.

Goetze, C., 1978. Mechanisms of creep in olivine, *Phil. Trans. R. Soc.,* **288**(1350), 99–119.

Hutko, A.R., Lay, T., Garner, E.J. & Revenaugh, J., 2006. Seismic detection of folded, subducted lithosphere at the core-mantle boundary, *Nature,* **441**, 333–336.

Katayama, I. & Karato, S.I., 2008. Low-temperature, high-stress deformation of olivine under water-saturated conditions, *Phys. Earth Planet. Inter.,* **168**(3–4), 125–133.

Kirby, S.H. & Kronenberg, A.K., 1984. Deformation of clinopyroxenite – evidence for a transition in flow mechanisms and semibrittle behavior, *J. geophys. Res.,* **89**(NB5), 3177–3192.

Kocher, T., Schmalholz, S.M. & Mancktelow, N.S., 2006. Impact of mechanical anisotropy and power-law rheology on single layer folding, *Tectonophysics,* **421**, 71–87.

Kohlstedt, D.L., Evans, B. & Mackwell, S.J., 1995. Strength of the lithosphere – constraints imposed by laboratory experiments, *J. geophys. Res.,* **100**(B9), 17587–17602.

Kronenberg, A.K., Kirby, S.H. & Pinkston, J., 1990. Basal slip and mechanical anisotropy of biotite, *J. geophys. Res.,* **95**(B12), 19257–19278.

Molnar, P. & Jones, C.H., 2004. A test of laboratory based rheological parameters of olivine from an analysis of late Cenozoic convective removal of mantle lithosphere beneath the Sierra Nevada, California, USA, *Geophys. J. Int.,* **156**, 555–564.

Montesi, L.G.J. & Zuber, M.T., 2002. A unified description of localization for application to large-scale tectonics, *J. geophys. Res.,* **107,** doi:10.1029/2001JB000465.

Montesi, L.G.J. & Zuber, M.T., 2003. Spacing of faults at the scale of the lithosphere and localization instability: 2. Application to the Central Indian Basin, *J. geophys. Res.,* **108,** doi:10.1029/2002JB001924.

Neurath, C. & Smith, R.B., 1982. The effect of material properties on growth rates of folding and boudinage: experiments with wax models, *J. Struct. Geol.,* **4**, 215–229.

Ramberg, H., 1955. Natural and experimental boudinage and pinch-and-swell structures, *J. Geol.,* **63,** 512–526.

Ricard, Y. & Froidevaux, C., 1986. Stretching instabilities and lithospheric boudinage, *J. geophys. Res.,* **91**(B8), 8314–8324.

Rutter, E.H., 1974. Influence of temperature, strain rate and interstitial water in experimental deformation of calcite rocks, *Tectonophysics,* **22**(3–4), 311–334.

Schmalholz, S.M., Podladchikov, Y.Y. & Burg, J.-P., 2002. Control of folding by gravity and matrix thickness: implications for large-scale folding, *J. geophys. Res.,* **107**(B1), doi:10.1029/2001JB000355.

Schmalholz, S.M., Schmid, D.W. & Fletcher, R.C., 2008. Evolution of pinch-and-swell structures in a power-law layer, *J. Struct. Geol.,* **30,** 649–663.

Schmeling, H., 2010. Dynamic models of continental rifting with melt generation, *Tectonophysics,* **480,** 33–47.

Schmid, S.M., Paterson, M.S. & Boland, J.N., 1980. High-temperature flow and dynamic recrystallization in Carrara marble, *Tectonophysics,* **65**(3–4), 245–280.

Shea, W.T. & Kronenberg, A.K., 1993. Strength and anisotropy of foliated rocks with varied mica contents, *J. Struct. Geol.,* **15**(9–10), 1097–1121.

Sherwin, J. & Chapple, W.M., 1968. Wavelengths of single layer folds: a comparison between theory and observation, *Am. J. Sci.,* **266,** 167–179.

Smith, R.B., 1977. Formation of folds, boudinage, and mullions in non-Newtonian materials, *Geol. Soc. Am. Bull.,* **88**(2), 312–320.

Trepmann, C.A. & Stockhert, B., 2009. Microfabric of folded quartz veins in metagreywackes: dislocation creep and subgrain rotation at high stress, *J. Metamorphic Geol.,* **27**(8), 555–570.

Tsenn, M.C. & Carter, N.L., 1987. Upper limits of power law creep of rocks, *Tectonophysics,* **136**(1–2), 1–26.